Chemomechanical regulation of EZH2 localization controls epithelial-mesenchymal transition

Jessica L. Sacco[1], Zachary T. Vaneman[1], Ava Self[1,3], Elix Sumner[1,4], Stella Kibinda[1], Chinmay S. Sankhe[1,5], Esther W. Gomez[1,2*]

[1]Department of Chemical Engineering, The Pennsylvania State University, University Park, PA, USA

[2]Department of Biomedical Engineering, The Pennsylvania State University, University Park, PA, USA

Present address:

[3]Department of Chemical Engineering, Massachusetts Institute of Technology, Cambridge, MA, USA

[4]Flathead Valley Community College, Kalispell, MT, USA

[5]Abigail Wexner Research Institute, Nationwide Children's Hospital, Columbus, OH, USA

*Corresponding author: ewg10@psu.edu

Running Title: Chemomechanical regulation of EZH2

Keywords: histone modification, methyltransferase, transforming growth factor, polycomb repressive complex, cell contractility, matrix stiffness

Summary statement

Stiff matrices promote transforming growth factor β1-induced epithelial-mesenchymal transition via regulation of nuclear localization of enhancer of zeste homolog 2.

Abstract

The methyltransferase enhancer of zeste homolog 2 (EZH2) regulates gene expression and aberrant EZH2 expression and signaling can drive fibrosis and cancer. However, it is not clear how chemical and mechanical signals are integrated to regulate EZH2 and gene expression. We show that culture of cells on stiff matrices in concert with transforming growth factor (TGF)-β1 promotes nuclear localization of EZH2 and an increase in the levels of the corresponding histone modification, H3K27me3, thereby regulating gene expression. EZH2 activity and expression are required for TGFβ1- and stiffness-induced increases in H3K27me3 levels as well as for morphological and gene expression changes associated with epithelial-mesenchymal transition (EMT). Inhibition of Rho associated kinase (ROCK) or myosin II signaling attenuates TGFβ1-induced nuclear localization of EZH2 and decreases H3K27me3 levels in cells cultured on stiff substrata, suggesting that cellular contractility, in concert with a major cancer signaling regulator TGFβ1, modulates EZH2 subcellular localization. These findings provide a contractility-dependent mechanism by which matrix stiffness and TGFβ1 together mediate EZH2 signaling to promote EMT.

Introduction

During fibrosis and cancer, the stiffness of the affected tissue significantly increases (Brown et al., 2013; Levental et al., 2010; Liu et al., 2010; Lopez et al., 2011; Plodinec et al., 2012). Increased matrix stiffness precedes liver fibrosis in rat models (Georges et al., 2007) and increased breast tissue stiffness is associated with breast cancer risk (Boyd et al., 2014), suggesting that matrix stiffness may play a causal role in epithelial disease progression. In addition, matrix stiffness regulates cellular processes implicated in disease progression including proliferation, differentiation, epithelial-mesenchymal transition (EMT), and apoptosis (Engler et al., 2006; Leight et al., 2012; O'Connor et al., 2015; Wang et al., 2000). Transforming growth factor (TGF)-β is a multi-functional cytokine that is important for maintaining homeostasis and regulating normal physiological processes, but if misregulated can promote epithelial diseases such as fibrosis and cancer (Elliot and Blobe, 2005; Sankhe et al., 2023). While previous studies have identified a regulatory role for matrix stiffness in the control of TGFβ-induced cell behavior and fate decisions, mechanistically how matrix mechanics mediate cell signaling and gene expression in response to TGFβ to promote disease progression has not been fully elucidated.

Global gene regulation is a dynamic process that plays an important role in EMT, and transcription is mediated by chromatin regulators including Enhancer of Zeste Homolog 2 (EZH2). EZH2, a methyltransferase that catalyzes the tri-methylation of histone 3 lysine 27 (H3K27me3) (Duan et al., 2020), regulates gene expression during normal and pathological processes. EZH2-knockout mouse embryos are deformed and die at an early developmental stage, suggesting that EZH2 is required for normal development (Shen et al., 2008). Aberrant expression of EZH2 correlates with progression of fibrosis and cancer, as EZH2 is hyperactivated in multiple types of cancers and is overexpressed in fibrosis (Grindheim et al., 2019; Simon and Lange, 2008; Tsou et al., 2019). EZH2 can serve as both a suppressor and an activator of genes associated with EMT (Cao et al., 2008; Han et al., 2016; Song et al., 2019) and apoptosis (Zhang et al., 2014) and plays a role in regulating both of these cellular processes. Indeed, EZH2 overexpression promotes EMT (Zhang et al., 2017), while EZH2 inhibition and knockdown reduce vimentin and increase E-cadherin expression in endometriotic epithelial (Zhang et al., 2017), liver cancer (Liu et al., 2010), and laryngeal cancer (Liu et al., 2010) cells and attenuate TGFβ1-induced EMT in retinal pigment epithelial cells (Andrews et al., 2019). Furthermore, EZH2 and H3K27me3 levels are elevated at the E-cadherin gene promoter in prostate cancer cells (Cao et al., 2008) and TGFβ1 treatment increases EZH2 levels at the E-cadherin gene promoter in retinal pigment epithelial cells (Andrews et al., 2019). These previous findings provide evidence that EZH2 regulates gene expression and epithelial disease progression; however, the synergistic impact of chemical and physical properties of the microenvironment on EZH2 signaling is unknown.

Here, we synthesized hydrogels with stiffnesses that mimic healthy and diseased mammary tissue and utilized this platform to examine the impact of matrix stiffness and TGFβ1 on EZH2, H3K27 methylation, and gene expression. We find that TGFβ1 treatment promotes EZH2 nuclear localization in cells cultured on stiff, but not soft substrata, and increased nuclear localization of EZH2 correlates with higher H3K27me3 levels. Inhibition and knockdown of EZH2 attenuates TGFβ1-induced morphology and gene expression changes associated with EMT in cells cultured on stiff substrata. Furthermore, inhibition of Rho associated kinase (ROCK) and myosin II reduces TGFβ1-induced EZH2 nuclear localization and H3K27me3 levels in cells cultured on stiff substrata. These results suggest a cell contractility-dependent mechanism by which TGFβ1 and matrix stiffness induce an EMT-associated transcriptional profile and phenotype via control of EZH2 subcellular localization.

Results

Matrix stiffness and TGFβ1 regulate EZH2 subcellular localization and H3K27me3 levels

Cancer and fibrosis progression are accompanied by changes in the mechanical properties of the affected tissue and elevation of the level and activity of TGFβ (Sankhe et al., 2023). The methyltransferase EZH2 is elevated in metastatic cancer and fibrosis (Cao et al., 2008; Kleer et al., 2003; Tsou et al., 2019; Varambally et al., 2002) and EZH2 is regulated by TGFβ1 (Andrews et al., 2019; Le et al., 2021); however, how matrix stiffness impacts EZH2 signal transduction is not clear. To mimic the mechanical properties of mammary tissue during disease progression, hydrogels were synthesized to have Young's moduli similar to healthy breast tissue (300 Pa) and an average breast tumor (6300 Pa) (Lopez et al., 2011; Plodinec et al., 2012). To examine EZH2 signaling in response to matrix stiffness and TGFβ1, normal murine mammary gland (NMuMG) epithelial cells were cultured on fibronectin-coated hydrogels and treated with TGFβ1. Immunofluorescence staining was utilized to examine the subcellular localization of EZH2. For cells cultured on soft substrata (300 Pa), EZH2 localization is pancellular and it is found both in the nucleus and cytoplasm in TGFβ1 and control vehicle treated cells (Fig. 1A). In contrast, for cells cultured on stiff substrata (6300 Pa), EZH2 localizes primarily to the cell nucleus when cells are treated with TGFβ1, while cells treated with control vehicle show both nuclear and cytoplasmic localization of EZH2. Quantification of the nuclear to cytoplasmic ratio of EZH2 from immunofluorescence images revealed that when cells are cultured on soft substrata the nuclear and cytoplasmic levels of EZH2 are comparable for control vehicle and TGFβ1 treated cells (Fig. 1B). In contrast, when cultured on stiff substrata, cells exhibit a significantly higher (2.2 fold, $p<0.01$) nuclear to cytoplasmic ratio of EZH2 following treatment with TGFβ1 than when

treated with control vehicle. Furthermore, TGFβ1 treatment promotes a significant increase (1.4 fold, $p<0.05$) in the nuclear to cytoplasmic ratio of EZH2 in cells cultured on stiff compared to soft matrices.

Western blots of whole cell lysates for EZH2 reveal that NMuMG cells cultured on stiff substrata show an approximately 20% decrease ($p<0.01$) in total EZH2 levels in comparison to when they are cultured on soft substrata (Fig. 1C,D). Treatment with TGFβ1 significantly decreases (1.2 fold, $p<0.05$) the total level of EZH2 in cells cultured on soft substrata and slightly, though not significantly, decreases total EZH2 levels in cells cultured on stiff substrata in comparison to control vehicle treated cells. Western blotting of cytoplasmic protein extracts revealed that EZH2 cytoplasmic levels are highest in control vehicle treated cells cultured on stiff substrata, and TGFβ1 treatment significantly reduces (7.7 fold, $p<0.01$) these levels (Fig. 1C,E). Western blotting of nuclear extracts revealed that nuclear EZH2 levels are significantly higher (greater than 2 fold, $p<0.05$) in cells cultured on stiff substrata and treated with TGFβ1 in comparison to all other experimental conditions (Fig. 1C,F). Together, the imaging and western blotting results demonstrate that when cells are cultured on stiff substrata, TGFβ1 treatment promotes EZH2 nuclear localization and significantly increases nuclear levels of EZH2; in contrast, cells cultured on soft substrata do not show significant subcellular redistribution of EZH2 in response to TGFβ1.

EZH2 is a methyltransferase that is responsible for tri-methylating histone 3 lysine 27 (H3K27) (Duan et al., 2020). To confirm increased methyltransferase activity of EZH2 in cells cultured on stiff substrata following TGFβ1 treatment in comparison to other treatment conditions we examined H3K27me3 levels. Immunofluorescence staining (Fig. S1A,B) shows that on soft substrata, H3K27me3 levels remain unchanged regardless of treatment condition, while TGFβ1 induces a significant increase in H3K27me3 levels in cells cultured on stiff substrata when compared to control vehicle treated cells cultured on stiff substrata (1.5 fold, $p<0.05$) and to TGFβ1 treated cells cultured on soft substrata (2.4 fold, $p<0.05$). Consistent with the staining results, western blotting similarly shows that H3K27me3 levels remain unchanged regardless of treatment condition in cells cultured on soft substrata, but TGFβ1 treatment significantly increases H3K27me3 levels in cells cultured on stiff substrata compared to control treated cells cultured on stiff substrata (2.8 fold, $p<0.05$) and compared to TGFβ1 treated cells cultured on soft substrata (3.9 fold, $p<0.01$) (Fig. 1G,H). Similar results are observed by immunofluorescence staining for Madin-Darby canine kidney (MDCK) epithelial cells, suggesting that matrix stiffness- and TGFβ1-induced increase in H3K27me3 levels is not cell type specific (Fig. S1C,D). Together, these results suggest that matrix stiffness and TGFβ1 coordinate to regulate the global levels of H3K27mMe3 in cells, which is likely mediated by control of EZH2 subcellular localization rather than by changes in EZH2 expression level.

Matrix stiffness and TGFβ1 mediate phosphorylation of EZH2

EZH2 phosphorylation at T311 and T367 correlates with its nuclear localization in some cell types (Ghate et al., 2023; Le et al., 2021; McMullen et al., 2021). We used western blotting to determine whether TGFβ1 induces EZH2 phosphorylation in cells cultured on a stiff matrix. TGFβ1 treated cells cultured on 6300 Pa compared to 300 Pa substrata show a significant increase in EZH2 molecular weight (4.0 fold, $p<0.05$) indicated by an upward shift of the bands of the western blot (Fig. 2A,B). Treatment of the whole cell lysate with alkaline phosphatase attenuates the observed increase in EZH2 molecular weight in cells cultured on 6300 Pa substrata and treated with TGFβ1 (5.1 fold, $p<0.001$) (Fig. 2A,B), suggesting that TGFβ1 treatment promotes phosphorylation of EZH2 in cells cultured on 6300 Pa substrata. Western blotting was also used to examine the levels of EZH2 phosphorylation at Threonine 311 (pEZH2-T311). TGFβ1 treated cells cultured on 6300 Pa substrata exhibit significantly higher levels of pEZH2-T311 compared to control treated cells cultured on 6300 Pa substrata (3.4 fold, $p<0.01$) and compared to TGFβ1 treated cells cultured on 300 Pa substrata (5.3 fold, $p<0.01$) (Fig. 2C,D). These results suggest that TGFβ1 and a stiff matrix promote phosphorylation of EZH2 at T311. In addition, we examined the subcellular localization of pEZH2-T311 using immunofluorescence staining. In control treated cells cultured on either 300 or 6300 Pa substrata, pEZH2-T311 is pancellular with nuclear:cytoplasm ratios around 0.25 (Fig. 2E,F). TGFβ1 treated cells cultured on 300 Pa substrata appear to have pancellular pEZH2-T311 localization with a nuclear:cytoplasm ratio of 0.23 (Fig. 2E,F). In contrast, TGFβ1 treated cells cultured on 6300 Pa substrata have significantly increased nuclear:cytoplasm ratio of pEZH2-T311 compared to control treated cells cultured on 6300 Pa substrata (4.0 fold, $p<0.0001$) and compared to TGFβ1 treated cells cultured on 300 Pa substrata (4.1 fold, $p<0.0001$) (Fig. 2E,F). We also examined phosphorylation of EZH2 at T367 as a function of matrix stiffness and TGFβ1 treatment. In control treated cells cultured on either 300 Pa or 6300 Pa substrata and in TGFβ1 treated cells cultured on 300 Pa substrata, pEZH2-T367 appears to have pancellular localization, and nuclear:cytoplasm ratios are below 0.33 (Fig. 2G,H). However, TGFβ1 treated cells cultured on 6300 Pa substrata have a significantly higher nuclear:cytoplasmic ratio of pEZH2-T367 compared to control treated cells cultured on 6300 Pa substrata (5.0 fold, $p<0.0001$) and compared to TGFβ1 treated cells cultured on 300 Pa substrata (3.3 fold, $p<0.0001$) (Fig. 2G,H). These results suggest that the combination of a stiff matrix and TGFβ1 stimulation promotes increased pEZH2-T311 and pEZH2-T367 levels and nuclear localization.

EZH2 activity and expression are required for TGFβ1-induced EMT in cells cultured on stiff substrata

Histone modifications, such as H3K27me3, can influence gene expression by altering chromatin accessibility. Thus, we hypothesized that regulation of EZH2 subcellular localization by matrix stiffness may mediate TGFβ1-induced changes in cell morphology and in the expression of genes associated with EMT. To test whether high global levels of H3K27me3 in TGFβ1-treated cells cultured on stiff matrices are

associated with EMT and require EZH2 activity, we used the inhibitor Deazaneplanocin A (DZNep), which inhibits EZH2 methyltransferase activity by inhibiting S-adenosylmethionine-dependent methyltransferase. To first confirm that DZNep inhibits methyltransferase activity in our system, cells were treated with DZNep prior to TGFβ1 stimulation and H3K27me3 levels were monitored. Immunofluorescence staining (Fig. S2A,B) revealed that DZNep treatment attenuates the TGFβ1-induced increase in H3K27me3 levels in cells cultured on stiff substrata (1.8 fold, $p<0.01$). Western blotting confirmed immunofluorescence staining results, showing that treatment with DZNep significantly reduces H3K27me3 levels (2.8 fold, $p<0.001$) in TGFβ1 treated cells in comparison to treatment with TGFβ1 and the control vehicle for cells cultured on stiff substrata (Figure 3A,B). These results verify that DZNep treatment reduces the global levels of H3K27me3 in TGFβ1-treated cells cultured on stiff matrices.

Cells that undergo EMT experience significant morphological changes including increased spreading and elongation as well as cytoskeletal reorganization (Kalluri and Weinberg, 2009). We have previously shown that matrix stiffness regulates TGFβ1-induced morphological changes and cytoskeletal reorganization (O'Connor et al., 2015), and we sought to determine whether EZH2 activity contributes to these observations. To examine cell morphology, we quantified cell spread area and aspect ratio in cells cultured on soft and stiff substrata that were treated with DZNep prior to TGFβ1 stimulation. Consistent with previous reports, we find that when NMuMG cells are cultured on soft substrata, the cells are rounded and associate with neighboring cells, and treatment with TGFβ1 and DZNep does not induce a change in cell morphology (Figs 3C-E and S2C). In contrast, when cells are cultured on stiff substrata, treatment with TGFβ1 promotes increased cell spreading in comparison to treatment with control vehicle. Furthermore, treatment with DZNep significantly reduces cell spread area (1.8 fold, $p<0.0001$) and aspect ratio (1.9 fold, $p<0.0001$) in TGFβ1 treated cells cultured on stiff substrata (Figs 3C-E and S2C). Interestingly, treatment with DZNep does not block TGFβ1-induced cytoskeletal reorganization in cells cultured on stiff substrata (Fig. S2D). These findings indicate that reducing EZH2 activity attenuates TGFβ1-induced increases in cell spreading and elongation in cells cultured on stiff substrata, suggesting that EZH2 may play a role in stiffness mediated TGFβ1-induced EMT.

To examine the role of EZH2 in the regulation of gene expression in response to matrix stiffness and TGFβ1, we monitored the expression of epithelial and mesenchymal markers following EZH2 inhibition. Immunofluorescence staining of cells cultured on soft substrata revealed that the epithelial marker E-cadherin localizes to cell-cell junctions in all treatment conditions (Fig. 3C). On stiff substrata, cells treated with TGFβ1 exhibit reduced E-cadherin expression and there is an increase in the percentage of cells expressing αSMA (13 fold, $p<0.001$). We observe αSMA expression in a subpopulation of cells (~15%), suggesting that cells exhibit differential responses to TGFβ1. DZNep treatment of cells cultured on stiff

substrata attenuates TGFβ1-induced loss of E-cadherin and significantly reduces the percentage of cells expressing αSMA (8.7 fold, $p<0.001$; Fig. 3C,F). Western blotting revealed that E-cadherin protein levels do not change significantly with TGFβ1 treatment when cells are cultured on soft substrata (Fig. 3G,H). For cells cultured on stiff substrata, treatment with TGFβ1 promotes a decrease in the levels of E-cadherin (2.7 fold, $p<0.001$) and an increase in the levels of αSMA (10.3 fold, $p<0.0001$), N-cadherin (1.9 fold, $p<0.0001$), and vimentin (1.9 fold, $p<0.0001$) in comparison to treatment with control vehicle (Fig. 3G-K). Treatment with DZNep attenuates the TGFβ1-mediated changes in E-cadherin, αSMA, N-cadherin, and vimentin levels. Together, these findings suggest that EZH2 activity regulates the expression of EMT associated genes in cells that encounter a stiff matrix and TGFβ1. Furthermore, because EZH2 inhibition with DZNep does not impact cytoskeletal changes, this suggests that the EMT phenotype is promoted by transcriptional reprogramming downstream of EZH2.

DZNep inhibits EZH2 methyltransferase activity indirectly by inhibiting S-adenosylmethionine-dependent methyltransferase. Because of this, DZNep inhibition could have off-target effects (Fujiwara et al., 2014; Miranda et al., 2009). To specifically target EZH2, we depleted EZH2 protein levels using an siRNA targeting EZH2 (Fig. 4A,B) to examine whether EZH2 expression, in addition to its activity, is required for matrix stiffness mediated cell morphology alterations, cytoskeletal reorganization, and EMT-associated gene expression changes in response to TGFβ1. Immunofluorescence staining (Fig. S3A,B) and western blotting (Fig. 4C,D) revealed that EZH2 knockdown attenuates the observed TGFβ1-induced increase in H3K27me3 levels in cells cultured on stiff substrata. Furthermore, EZH2 knockdown reduces TGFβ1-mediated changes in cell spread area and aspect ratio in cells cultured on stiff substrata in comparison to cells transfected with a non-targeting control siRNA (Figs 4E-G and S3C). Knockdown of EZH2, however, does not appear to impact TGFβ1-induced cytoskeletal reorganization in cells cultured on stiff substrata (Fig. S3D).

Examination of the levels of EMT markers by immunofluorescence staining showed that when cells are cultured on stiff substrata, TGFβ1 reduces E-cadherin levels and significantly increases the percentage of cells expressing αSMA (10 fold, $p<0.001$) in cells transfected with control siRNA (Fig. 4E,H). Consistent with this, western blotting reveals a reduction in E-cadherin levels (2.7 fold, $p<0.05$) and an increase in αSMA (8.3 fold, $p<0.001$), N-cadherin (2.1 fold, $p<0.01$), and vimentin (2.0 fold, $p<0.01$) protein levels in cells transfected with the control siRNA following treatment with TGFβ1 (Fig. 4I-M). EZH2 knockdown slightly, though not significantly, reduces TGFβ1-induced loss of E-cadherin in cells cultured on both soft and stiff substrata (Fig. 3I,J), and significantly reduces TGFβ1-induced gain in αSMA (5.3 fold, $p<0.001$) and vimentin (1.7 fold, $p<0.01$) protein levels in cells cultured on stiff substrata (Fig. 4I,K,M). EZH2 knockdown reduces TGFβ1-induced gain in N-cadherin protein levels in cells cultured on stiff substrata,

though not significantly (Fig. 4L). These findings suggest that both EZH2 expression and activity are required for matrix stiffness and TGFβ1-induced changes in the levels of H3K27me3 and some EMT-associated proteins. Moreover, these results indicate that a stiff matrix and TGFβ1 signaling promote nuclear localization of EZH2, which elevates H3K27me3 levels and promotes gene expression changes associated with EMT.

Cytoskeletal contractility mediates TGFβ1-induced changes in the subcellular localization of EZH2 on stiff substrata

Given that inhibition of ROCK, a downstream target of RhoA, prevents TGFβ1-induced αSMA expression and EMT in cells cultured on stiff matrices (O'Connor et al., 2015), we hypothesized that cytoskeletal contractility may regulate EZH2 subcellular localization. Cells were cultured on hydrogels of varying stiffness and treated with TGFβ1 and the ROCK inhibitor Y27632. Immunofluorescence staining shows similar EZH2 nuclear and cytoplasmic localization in cells cultured on soft substrata across all treatment conditions, with the ratio of nuclear and cytoplasmic levels being near a value of one (Fig. 5A,B). In cells cultured on stiff substrata, EZH2 localizes primarily to the nucleus when cells are treated with TGFβ1, while treatment with Y27632 reduces TGFβ1-induced EZH2 nuclear to cytoplasmic levels (2.1 fold, $p<0.001$) (Fig. 5A,B). Western blotting revealed that on soft substrata, EZH2 protein levels are similar in cytoplasmic and nuclear extracts across treatment conditions (Fig. 5C-E). For cells cultured on stiff substrata, treatment with Y27632 and TGFβ1 promotes a significant increase (3 fold, $p<0.05$) in cytoplasmic EZH2 levels in comparison to treatment with TGFβ1 alone (Fig. 5C,D). Furthermore, treatment with Y27632 and TGFβ1 significantly reduces (4.4 fold, $p<0.01$) the levels of nuclear EZH2 in comparison to treatment with TGFβ1 alone for cells cultured on stiff substrata (Fig. 5C,E).

To confirm that inhibition of ROCK signaling impacts EZH2 activity, we examined H3K27me3 levels using immunofluorescence staining and western blotting. Western blotting showed that for cells cultured on soft substrata, H3K27me3 levels are low across all treatment conditions, while on stiff substrata Y27632 treatment significantly reduces H3K27me3 levels (2.4 fold, $p<0.01$) in TGFβ1 treated cells in comparison to treatment with TGFβ1 alone (Fig. 5F,G). Similar trends were observed by immunofluorescence staining analysis (Fig. S4A,C). Treatment with blebbistatin, a myosin II inhibitor, has been shown to attenuate matrix stiffness- and TGFβ1-induced EMT (O'Connor et al., 2015). Blebbistatin and TGFβ1 treatment also reduces H3K27me3 levels and EZH2 nuclear localization in comparison to treatment with TGFβ1 alone in cells cultured on stiff substrata (Fig. S4B,D-H). These results demonstrate that RhoA/ROCK signaling and myosin II regulate EZH2 subcellular localization and H3K27me3 levels in response to matrix stiffness and TGFβ1. Taken together, these results provide a cell contractility-mediated mechanism for understanding how EZH2 contributes to the regulation of TGFβ1-induced EMT (Fig. 6).

Discussion

Recent studies suggest that microenvironmental mechanical cues regulate chromatin reorganization and histone 3 acetylation and methylation to mediate transcription. For example, compressive load, which varies during tumor growth, increases chromatin condensation and H3K27me3 levels, promotes nuclear localization of histone deacetylase 3 (HDAC3), and reduces transcriptional activity (Damodaran et al., 2018). Cells can also be subjected to biaxial strain in the tumor microenvironment. Mechanical biaxial strain has been found to induce global chromatin rearrangement and to promote transcriptional repression by increasing H3K27me3 levels (Le et al., 2016). In addition, matrix stiffness regulates chromatin spatial organization, condensation state, and accessibility (Heo et al., 2023; Stowers et al., 2019; Walker et al., 2022). MCF10A breast epithelial cells cultured in stiff (2000 Pa) matrices have significantly more accessible chromatin regions than cells cultured in soft (100 Pa) matrices (Stowers et al., 2019). For mesenchymal stem cells, the total number of H3K27me3 localizations per unit area of the entire nucleus does not show differences as a function of matrix stiffness, however, cells cultured on soft substrata exhibit higher levels of H3K27me3 localization at the nuclear periphery than cells cultured on stiffer substrata suggesting higher levels of heterochromatin structures and transcriptional repression (Heo et al., 2023). We find that H3K27me3 levels do not vary in mammary epithelial cells as a function of matrix stiffness when treated with control vehicle. In contrast, treatment with TGFβ1 promotes a significant increase in the levels of H3K27me3 in cells cultured on stiff substrata in comparison to cells cultured on soft substrata. Given that H3K27me3 is typically associated with heterochromatin and downregulation of a large number of epithelial markers occurs during EMT, these data suggest that stiff substrata may enhance TGFβ1-induced transcriptional repression of epithelial-associated genes via the repressive H3K27me3 mark. Future studies examining the nanoscale reorganization of chromatin and localization of the H3K27me3 mark as a function of matrix mechanical properties and growth factor stimulation may shed light on the interplay between physical and chemical cues in the regulation of chromatin organization and gene expression.

In this study, we found that matrix stiffness regulates EZH2 subcellular localization in response to stimulation with TGFβ1. On stiff, but not soft substrata, TGFβ1 increases EZH2 nuclear localization and H3K27me3 levels. Previous studies have shown that EZH2 is present in the cytoplasm and nucleus of benign and malignant prostate cancer cells, and both cytoplasmic and nuclear EZH2 is increased in prostate cancer cells compared to benign prostate cells (Bryant et al., 2008). In addition, EZH2 total protein level and nuclear localization is significantly higher in invasive breast carcinoma compared to benign breast lesions, which exhibit no nuclear localized EZH2 (Pang et al., 2012). Increased matrix stiffness (Levental et al., 2010; Lopez et al., 2011) and EMT (Ye and Weinberg, 2015) correlate with a mesenchymal phenotype

and increased tumor cell invasion; thus, matrix stiffness may regulate increased nuclear levels of EZH2 observed in invasive breast cancers reported in the literature. Our results support this, as we observe increased nuclear localization of EZH2 and increased mesenchymal features in TGFβ1-treated mammary epithelial cells cultured on stiff substrata. Moreover, reports demonstrate that EZH2 localization also varies as a function of tumor stage and type. Cytoplasmic EZH2 is observed in 16% of invasive carcinomas and is associated with estrogen receptor negative and triple negative tumors, while nuclear EZH2 is associated with HER2 overexpression and higher tumor grade (Pang et al., 2012). Further studies are needed to delineate the role of matrix stiffness and other mechanical cues, such as elevated solid compressive stress and increased interstitial fluid pressure associated with tumors, in regulation of the subcellular localization of EZH2 in normal cells from a variety of tissues as well as in diseased cells from different types, stages, and grades of cancers.

Nuclear localization of EZH2 has been previously demonstrated to correlate with its phosphorylation state (Ghate et al., 2023; Le et al., 2021; McMullen et al., 2021). Cytoplasmic pEZH2 T367 is significantly higher in squamous compared to mesenchymal and spindle subtypes of metaplastic carcinoma, while high nuclear pEZH2 T367 correlates to mesenchymal subtypes (McMullen et al., 2021). In our study we find that EZH2 localizes in both the cytoplasm and nucleus in cells exhibiting an epithelial phenotype, and pEZH2 T367 levels and nuclear localization are higher in cells exhibiting a mesenchymal phenotype. Another study found that in EZH2-depleted SW620 colon cancer cells, overexpression of an EZH2 mutant with an aspartic acid substitution that mimics T367 phosphorylation restores H3K27me3 levels and promotes complete EZH2 nuclear localization (Ghate et al., 2023). The mutant had more efficient nuclear accumulation of EZH2 and higher H3K27me3 levels than EZH2 wild-type cells suggesting that pEZH2 T367 promotes EZH2 nuclear stabilization (Ghate et al., 2023). Furthermore, TGFβ signaling has been shown to contribute to EZH2 phosphorylation and subcellular localization; TGFβ-induced nuclear translocation of transforming growth factor-β-activated kinase 1 (TAK1) promotes phosphorylation of EZH2 at T311 and releases EZH2 from the polycomb repressive complex 2 (PRC2) to establish a transcriptional complex of EZH2, RNA-polymerase II (POL2), and nuclear actin that promotes EMT. Inhibition of EZH2, TAK1, or nuclear actin influx attenuates TGFβ-induced fibroblast-myofibroblast transition (Le et al., 2021). EZH2 knockdown did not block TGFβ-induced actomyosin remodeling, while Y27632 attenuates TGFβ-induced formation of the EZH2-POL2-actin transcriptional complex (Le et al., 2021). Similarly, in our study, EZH2 inhibition and knockdown does not impact cytoskeletal reorganization, but RhoA/ROCK inhibition via Y27632 attenuates TGFβ1-induced gene expression. Thus, the EZH2-mediated gene expression changes that we see in our system in response to TGFβ1 and a stiff matrix may be a result of the EZH2-POL2-actin transcriptional complex assembled by phosphorylation of EZH2 at T311 by TGFβ-induced nuclear TAK1 observed in the abovementioned study. In our study, we find that

TGFβ1 promotes nuclear EZH2 to drive EMT in cells cultured on stiff substrata and this requires cellular contractility. Additional studies are necessary to gain further mechanistic insight into the regulation of EZH2 phosphorylation and nuclear localization by TGFβ1 and matrix stiffness.

Prior studies have found that EZH2 inhibition and knockdown reduces RhoA (Tripathi et al., 2021) and ROCK (Barsotti et al., 2015) activity and regulates actin polymerization (Bryant et al., 2008; Roy et al., 2012; Su et al., 2005). In contrast to these previous findings of EZH2 functioning upstream of RhoA/ROCK signaling to regulate actin polymerization, we find that both EZH2 inhibition and knockdown do not impact the structure of F-actin in cells cultured on both soft and stiff substrata (Figs S2D and S3D). Cells maintained cortical actin organization when cultured on soft substrata regardless of treatment and when cultured on stiff substrata and treated with the control vehicle. In cells cultured on stiff substrata, TGFβ1 treatment induced cytoskeletal reorganization and F-actin stress fiber structures in both DZNep and control vehicle treated cells and in cells transfected with both a control and an EZH2 siRNA. These results suggest that in our system, EZH2 is mainly functioning in the nucleus to regulate gene expression rather than upstream of RhoA/ROCK signaling to mediate actin polymerization. In our study, we used normal murine mammary gland cells, while the aforementioned studies utilized lung cancer, melanoma, and prostate cancer cells. The differences observed between our study and the studies mentioned above may be attributed to differences in cell type, and whether EZH2 functions upstream or downstream of RhoA/ROCK may be cell type-dependent. Interestingly, inhibition of myosin II with blebbistatin has been shown to attenuate strain-induced increase in H3K27me3 levels and transcriptional repression of PRC target genes (Le et al., 2016). Our results are consistent with this finding, as we show that myosin II is required for TGFβ1-induced increase of nuclear localization of EZH2 and H3K27me3 levels in response to increased matrix stiffness. These findings suggest that cytoskeletal contractility mediates EZH2 subcellular localization and signaling.

While EZH2 and the H3K27me3 mark are usually associated with transcriptional repression (Andrews et al., 2019; Cao et al., 2008; Le et al., 2016), there is some evidence that EZH2 (Gonzalez et al., 2014; Manning et al., 2015; Song et al., 2019) and H3K27me3 (Young et al., 2011) also correlate with gene activation. Thus, it is possible that EZH2 can act as both a repressor and an activator of EMT-associated genes. Indeed, EZH2 levels are elevated at the E-cadherin gene promoter in prostate cancer cells, resulting in E-cadherin gene repression (Cao et al., 2008; Han et al., 2016). In addition, Smad3 and EZH2 localize to the E-cadherin gene promoter to repress E-cadherin in TGFβ1-treated retinal epithelial cells (Andrews et al., 2019). Furthermore, EZH2 promotes αSMA expression by forming a transcriptional complex with Smad2 to bind to the ACTA2 gene promoter region in angiotensin II-induced fibroblast differentiation (Song et al., 2019). Previous studies have also found that EZH2 expression is required for Notch (Gonzalez et al., 2014; Manning et al., 2015) and SRF reporter activity and SRF transcription (Manning et al., 2015),

which are important signaling pathways involved in the regulation of αSMA expression and EMT (O'Connor et al., 2015; O'Connor et al., 2016). We find that increased matrix stiffness promotes a decrease in E-cadherin expression and an increase in αSMA protein expression (ACTA2 gene) in response to TGFβ1. This finding is consistent with RNA-seq and ATAC-seq results for valve interstitial cells which showed that the ACTA2 gene is associated with open chromatin regions in cells cultured on stiff substrata (Walker et al., 2022). We also find that inhibition and knockdown of EZH2 impacts the protein-level expression of E-cadherin and αSMA in mammary epithelial cells cultured on stiff substrata. These findings are consistent with previously published reports that show EZH2 plays a role in the regulation of both E-cadherin and αSMA gene expression and add to our understanding of the regulation of these EMT markers by matrix mechanical properties.

Previous studies have suggested a positive correlation between cell proliferation and high EZH2 levels in cancer cells (Bachmann et al., 2006; Yomtoubian et al., 2020) and that cancer cells cultured in a stiff microenvironment exhibit increased proliferation in comparison to when they are cultured within a soft environment (Sankhe et al., 2024; Schrader et al., 2011). We observe a decrease in total EZH2 levels with an increase in matrix stiffness for normal mammary epithelial cells (Fig. 1C,D), which is opposite to the expected trend in cell proliferation for an increase in matrix stiffness. In addition, we observe a further decrease in EZH2 levels in cells cultured on stiff matrices following TGFβ1 treatment in comparison to treatment with control vehicle. Given that TGFβ1 has growth-inhibitory effects on normal epithelial cells (Kurokowa et al., 1987), this observed decrease in EZH2 levels may correlate with a decrease in proliferation. Further studies are needed to determine the relationship between cell proliferation and EZH2 levels as a function of TGFβ1 treatment and matrix stiffness.

During cancer progression, cells present in the tumor microenvironment, such as cancer associated fibroblasts, are responsible for increased deposition of extracellular matrix that promotes an increase in tissue stiffness (Martinez-Vidal et al., 2021). Increased collagen density, crosslinking, and fiber alignment is also associated with poor prognosis in cancer and together contribute to stiffening of the matrix (Conklin et al., 2011; Hanley et al., 2016; Provenzano et al., 2006). Therefore, collagen content and matrix crosslinking are potential targets for attenuating matrix stiffening and subsequent EZH2 nuclear translocation and activation of EMT. Furthermore, mechanical stresses in the tumor microenvironment can vary for individual cells, therefore EZH2 localization and H3K27me3 levels may vary at the single cell level within tumors. This could promote gene expression differences between cells within a tumor and contribute to intratumor heterogeneity. Thus, these findings could potentially inform future three-dimensional spatial single cell transcriptome studies.

A potential clinical implication of our findings is that cancer cells may exhibit differential sensitivities to EZH2 inhibition depending on the mechanical properties of their microenvironment. For example, cells in a soft microenvironment with low levels of nuclear EZH2 may be less sensitive to EZH2 inhibition than cells in a stiff microenvironment in the presence of TGFβ1 that have high nuclear EZH2 levels. Pharmacological inhibition of EZH2 significantly reduces the metastatic potential of luminal B breast cancer cells (Hirukawa et al., 2018). Furthermore, EZH2 inhibition enhances the efficacy of chemotherapy drugs in triple negative breast cancer cells of the mesenchymal subtype (Lehmann et al., 2021). One study identified a mesenchymal subtype of triple negative breast cancer cells with high EZH2 expression, enhanced invasion, and increased sensitivity to EZH2 inhibition compared to a luminal androgen receptor subtype (Yomtoubian et al., 2020). Another study found that synthetic gene activators that bind H3K27me3 can activate tumor suppressor genes and reduce triple-negative breast cancer invasion (Hong et al., 2023). These studies suggest that inhibition of EZH2 is a promising treatment approach for targeting cancer invasion and cancer cells of the mesenchymal subtype. Nonetheless, in order to improve therapeutic efficacy further studies are needed to elucidate how the mechanical properties of tumors may influence the epigenomic state and phenotype of cancer cells and the sensitivity of cancer cells to epigenetic treatments. Overall, our findings suggest that matrix stiffness, cell contractility, and EZH2 activity may be promising therapeutic targets in fibrosis and cancer.

Materials and methods

Cell culture

Normal murine mammary gland (NMuMG) epithelial cells (American Type Culture Collection ATCC CRL-1636) were authenticated by Genetica Cell Line Testing, a LabCorp brand, and cells tested negative for mycoplasma. NMuMG cells were grown in Dulbecco's Modified Eagle Medium (DMEM) with 10% (v/v) fetal bovine serum (FBS, Atlanta Biologicals), 0.01% gentamicin (Gibco), and 10 μg mL^{-1} insulin (Sigma Aldrich). Madin-Darby Canine Kidney (MDCK) epithelial cells (ATCC CCL-34) were grown in Eagle's Minimum Essential Medium (EMEM) with 10% FBS and 0.01% gentamicin. Cells were cultured in their respective medium in a 37°C incubator with 5% CO_2. Prior to all treatments, complete cell medium was replaced with reduced serum (2% FBS) medium. Cells were treated with 10 ng mL^{-1} of recombinant human TGFβ1 (R&D Systems) to induce EMT or a vehicle control (1 mg mL^{-1} bovine serum albumin in 4 mM HCl) 24 hours after cell seeding and were incubated for 48 hours prior to analysis. For inhibitor treatments, cells were treated with inhibitors for 1 hour prior to treatment with TGFβ1. The inhibitors blebbistatin (10 μM, Sigma Aldrich) and Y27632 (10 μM, Enzo Life Sciences) were diluted in dimethyl

sulfoxide (DMSO; Sigma), and for these experiments DMSO was used as the control vehicle. The inhibitor 3-Deazaneplanocin (DZNep; 1 μM, Sigma Aldrich) was diluted in deionized (DI) water, and DI water was used as the control vehicle for these experiments.

Polyacrylamide hydrogel synthesis

Polyacrylamide hydrogels of varying stiffness were synthesized using an adapted protocol (Tse and Engler, 2010). The hydrogels were composed of an acrylamide monomer (Sigma Aldrich) and bis-acrylamide crosslinker (Sigma Aldrich) in the presence of DI water. Polymerization was initiated using 10% w/v ammonium persulphate (Sigma Aldrich) and 0.05% v/v N, N, N', N'- tetramethylenediamine (TEMED, Sigma Aldrich). The polyacrylamide solutions were pipetted onto glass slides treated with 0.1 N sodium hydroxide (Sigma Aldrich), 2% v/v aminopropyltrimethoxysilane (APTMS, Sigma Aldrich), and glutaraldehyde (Sigma Aldrich) and left to polymerize for 30 minutes. Polyacrylamide hydrogels are not cell-adhesive, so they were activated and coated with the matrix protein fibronectin prior to cell seeding. Activation was achieved through treatment with 0.05 mM N-sulfosuccinimidyl-6-(4'-azido-2' nitrophenylamino) hexanoate (Sulfo-SANPAH, Thermo Scientific) in 0.5 M HEPES (pH 8.5) and exposure to 10 minutes of UV light in a CL-1000 Ultraviolet Crosslinker. This process was repeated twice. Activated hydrogels were rinsed with 0.5 M HEPES and incubated overnight with 0.1 μg mL^{-1} human fibronectin (BD Biosciences) at 4°C. Hydrogels were then thoroughly rinsed to remove excess fibronectin prior to plating cells.

siRNA transfections

Cells were transfected with small interfering RNA (siRNA) targeting EZH2 (#1: ID s65776, cat # 4390771; #2: ID s65777, cat # 4390771) and a Silencer Select Negative Control No. 1 siRNA (cat # 4390843) from Thermo Fisher Scientific. Briefly, cells were transfected at ~70% confluency using 10 μM siRNA and Lipofectamine RNAiMAX Transfection Reagent (Thermo) diluted in Opti-MEM medium (Thermo). The diluted siRNA and Lipofectamine were mixed in a 1:1 ratio and kept at room temperature for 5 minutes then added to the cells. Cells were plated to the hydrogels 24 hours after siRNA transfection, allowed to adhere to the hydrogels for 24 hours, and then treated with 10 ng mL^{-1} of recombinant human TGFβ1 (R&D Systems) or a vehicle control for 48 hours.

Immunofluorescence staining

To prepare samples for αSMA staining, cells were fixed with 1:1 methanol:acetone at -20°C. To prepare samples for staining of all other proteins, cells were fixed with 4% paraformaldehyde for 15 minutes at room temperature. Cells were permeabilized by treatment with 0.5% IGEPAL and 0.1% Triton X-100 at

room temperature for 10 minutes each then incubated for 1.5 hours at room temperature with a blocking buffer composed of 10% goat serum (Sigma Aldrich) in 1× phosphate buffered saline (PBS). Samples were incubated with the following primary antibodies at 4°C overnight: H3K27me3 (1:800; clone: C36B11, lot 8 & 19; Cell Signaling Technologies cat# 9733; RRID:AB_2616029), EZH2 (1:200; clone: D2C9, lot 9; Cell Signaling Technologies cat# 5246; RRID:AB_10694683), E-cadherin (1:200; clone: 24E10, lot 13 & 15; Cell Signaling Technologies cat# 3195; RRID:AB_2291471), αSMA (1:200; clone: 1A4, lot 0000162750; Sigma cat #A5228; RRID:AB_262054), phospho-EZH2 (Thr311) (1:100, clone: F1K1B, Cell Signaling Technologies cat # 70303; RRID:AB_3661652), and phospho-EZH2 (Thr367) (1:100, Thermo Scientific cat # PIPA5106225; RRID:AB_3661651). To remove unbound primary antibody, samples were rinsed with 1× PBS three times for 5 minutes with gentle shaking then incubated with Alexa Fluor-conjugated secondary antibodies (1:500 dilution, Life Technologies) for 1 hour at room temperature. To visualize F-actin, cells were incubated with Alexa-Fluor 594 phalloidin (Thermo) following the manufacturer's protocol. Samples were treated with Hoechst 33342 (1:10,000; Life Technologies) for 15 minutes at room temperature to visualize cell nuclei then mounted onto microscope slides with Fluoromount-G (Invitrogen) for imaging.

Microscopy and image analysis

Mounted samples were imaged using a 20× or 40× objective on a Nikon Eclipse Ti-E inverted fluorescence microscope equipped with a Photometrics CoolSNAP HQ^2 CCD camera using NIS-Elements AR 4.13.00 software. ImageJ version 1.53t software was used to measure integrated intensities of H3K27me3. The intensities were normalized to the control, and at least 50 nuclei were analyzed per sample. EZH2 subcellular localization was determined by ratioing the integrated nuclear and cytoplasmic intensities of EZH2 within the cells. The integrated nuclear intensities were determined by outlining the nuclear region of each cell. The integrated cytoplasmic intensities were determined by first outlining the whole cell and calculating whole cell integrated intensities, then subtracting the nuclear intensity from the whole cell intensity for each cell to obtain the cytoplasmic intensity of EZH2. ImageJ software was also used to measure cell spread area and aspect ratio (major/minor axis) for individual cells. When calculating the percentage of cells expressing αSMA, a cell was considered positive for αSMA based upon integrated staining intensity and the presence of clearly visible αSMA fibers.

Western blotting

Whole cell lysates were collected from cells using RIPA buffer (Thermo) with protease and phosphatase inhibitors. Histones were extracted using an adapted protocol (Shechter et al., 2007). Cytoplasmic and nuclear fractions of protein were extracted using a Subcellular Protein Fractionation Kit according to the

manufacturer's instructions (Thermo). Protein concentration was quantified using a Pierce BCA Protein Assay Kit (Thermo) or a Bradford protein assay using Coomassie blue reagent (Thermo). To examine molecular weight changes, whole cell lysates were incubated with 13 units of FastAP Thermosensitive Alkaline Phosphatase (1 U/μL, Thermo Fisher Scientific) for 1 hour at 37°C. Equal amounts of protein were separated on NuPAGE 4-12% Bis-Tris (Thermo) or NuPAGE 3-8% Tris-Acetate (Thermo) gels and transferred to polyvinyl difluoride (PVDF) or nitrocellulose membranes using an XCell SureLock Mini-Cell (Invitrogen). Membranes were blocked with 5% nonfat milk for an hour with gentle shaking and then incubated with the following primary antibodies overnight at 4°C: H3K27me3 (1:1000; clone: C36B11, lot 8 & 19; Cell Signaling Technologies cat# 9733; RRID:AB_2616029), EZH2 (1:1000; clone: D2C9, lot 9; Cell Signaling Technologies cat# 5246; RRID:AB_10694683), E-cadherin (1:1000; clone: 24E10, lot 13 & 15; Cell Signaling Technologies cat# 3195; RRID:AB_2291471), αSMA (1:1000; clone: 1A4, lot 0000162750; Sigma cat #A5228; RRID:AB_262054), vimentin (1:1000; clone: D21H3; Cell Signaling Technologies cat# 5741; RRID:AB_10695459), N-cadherin (1:1000; clone: 13A9; Cell Signaling Technologies cat# 14215S; RRID:AB_2798427), H3 (1:1000; clone: 1B1B2, lot 7 & 8; Cell Signaling Technologies cat# 14269; RRID:AB_2756816), phospho-EZH2 (Thr311) (1:1000, clone: F1K1B, Cell Signaling Technologies cat # 70303; RRID:AB_3661652), GAPDH (1:1000; clone: D16H11, lot 8; Cell Signaling Technologies cat# 5174; RRID:AB_10622025), and α-tubulin (1:1000; clone: DM1A, lot 2407525; Thermo cat# 62204; RRID:AB_1965960). Membranes were incubated with IRDye secondary antibodies (1:10,000; Li-COR Biosciences cat# 926-32210 and 925-68071; RRID: AB_621842 and AB_2721181) for 1 hour at room temperature with gentle shaking and then imaged using a Li-COR Odyssey CLx imager. ImageJ software was used to perform densitometric analysis of the blots. Normalized protein expression was quantified by dividing the intensity of the bands for the target protein by the intensity of the bands in the loading control. Relative protein levels were determined by dividing the normalized intensity of each sample by the intensity of the control for each experiment. Raw western blot images are shown in Fig. S5.

Statistical analysis

At least three trials with distinct samples were performed for each experiment. In the bar graphs, data are presented as mean ± standard error of the mean (s.e.m.). An analysis of variance followed by a Tukey-Kramer post hoc test using MATLAB was used to determine statistical differences. Data describing cell morphology are displayed as individual points overlaid by the mean ± s.e.m. with at least 150 cells analyzed across three different experiments. For data (cell spread area and aspect ratio measurements) that are not normally distributed as determined by the D'Agostino & Pearson, Anderson-Darling, Shapiro-Wilk, and Kolmogorov-Smirnov normality tests, the non-parametric Kruskal-Wallis with Dunn's post hoc analysis

was performed using the measurements from all 150 cells using GraphPad Prism version 9.5.1. Differences were considered significant for $p < 0.05$.

Acknowledgements

The authors would like to thank Dr. Justin Brown for use of the LI-COR Odyssey Imaging System for western blot imaging and Dr. Andrew Zydney for use of the TECAN Infinite 200 Pro microplate reader for protein quantification.

Competing interests

No competing interests declared

Funding

This work was supported by the National Science Foundation [CMMI-1751785 to E.W.G., EEC-1950639 to E.W.G.], NASA [PSGC to J.L.S.], and the Penn State Department of Chemical Engineering [Biofellowship to Z.T.V.]. E.S. was supported by EEC-1950639.

Data and resource availability

All relevant data and resources can be found within the article and its supplementary information.

References

Andrews, D., Oliviero, G., De Chiara, L., Watson, A., Rochford, E., Wynne, K., Kennedy, C., Clerkin, S., Doyle, B., GOdson, C. et al. (2019). Unraveling the transcriptional response of TGFβ: Smad3 and EZH2 constitute a regulatory switch that controls neuroretinal epithelial cell fate specification. *The FASEB Journal* **33**, 6667-6680.

Bachmann, I., Halvorsen, O., Collett, K., Stefansson, I., Straume, O., Haukaas, S., Salvesen, H., Otte, A. and Akslen, L. (2006). EZH2 expression is associated with high proliferation rate and aggressive tumor subgroups in cutaneous melanoma and cancers of the endometrium, prostate, and breast. *Journal of Clinical Oncology* **24**, 268-273.

Barsotti, A., Ryskin, M., Zhong, W., Zhang, W., Giannakou, A., Loreth, C., Diesl, V., Follettie, M., Golas, J., Lee, M. et al. (2015). Epigenetic reprogramming by tumor-derived EZH2 gain-of-function mutations promotes aggressive 3D cell morphologies and enhances melanoma tumor growth. *Oncotarget* **6**, 2928-2938.

Boyd, N., Li, Q., Melnichouk, O., Huszti, E., Martin, L., Gunasekara, A., Mawdsley, G., Yaffe, M. and Minkin, S. (2014). Evidence that breast tissue stiffness is associated with risk of breast cancer. *PLoS ONE* **9**, e100937.

Brown, A. C., Fiore, V. F., Sulchek, T. A. and Barker, T. H. (2013). Physical and chemical microenvironmental cues orthogonally control the degree and duration of fibrosis-associated epithelial-to-mesenchymal transition. *Journal of Pathology* **229**, 25-35.

Bryant, R., Winder, S., Cross, S., Hamdy, F. and Cunliffe, V. (2008). The polycomb group protein EZH2 regulates actin polymerization in human prostate cancer cells. *The Prostate* **68**, 255-263.

Cao, Q., Dhanasekaran, S., Kim, J., Mani, R., Tomlins, S., Mehra, R., Laxman, B., Cao, X., Yu, J., Kleer, C. et al. (2008). Repression of E-cadherin by the polycomb group protein EZH2 in cancer. *Oncogene* **27**, 7274-7284.

Conklin, M., Eickhoff, J., Riching, K., Pehlke, C., Eliceiri, K., Provenzano, P., Friedl, A. and Keely, P. (2011). Aligned collagen is a prognostic signature for survival in human breast carcinoma. *The American Journal of Pathology* **178**, 1221-1232.

Damodaran, K., Venkatachalapathy, S., Alisafaei, F., Radhakrishnan, A., Jokhun, D., Shenoy, V. and Shivashankar, G. (2018). Compressive force induces reversible chromatin condensation and cell geometry-dependent transcriptional response. *Molecular Biology of the Cell* **29**, 2969-3062.

Duan, R., Du, W. and Guo, W. (2020). EZH2: a novel target for cancer treatment. *Journal of Hematology and Oncology* **13**, 104.

Elliot, R. and Blobe, G. (2005). Role of transforming growth factor Beta in human cancer. *J. Clin. Oncol.* **23**, 2078-2093.

Engler, A., Sen, S., Sweeney, H. and Discher, D. (2006). Matrix elasticity directs stem cell lineage specification. *Cell* **126**, 677-689.

Fujiwara, T., Saitoh, H., Inoue, A., Kobayashi, M., Okitsu, Y., Katsuoka, Y., Fukuhara, N., Onishi, Y., Ishizawa, K., Ichinohasama, R. et al. (2014). 3-Deazaneplanocin A (DZNep), an inhibitor of

S-adenosylmethionine-dependent methyltransferase, promotes erythroid differentiation. *J Biol Chem* **289**, 8121-8134.

Georges, P., Hui, J., Gombos, Z., McCormick, M., Wang, A., Uemura, M., Mick, R., Janmey, P., Furth, E. and Wells, R. (2007). Increased stiffness of the rat liver precedes matrix deposition: implications for fibrosis. *American Journal of Physiology- Gastrointestinal and Liver Physiology* **293**, G1147-G1154.

Ghate, N., Kim, S., Shin, Y., Kim, J., Doche, M., Valena, S., Situ, A., Kim, S., Rhie, S., Lenz, H. et al. (2023). Phosphorylation and stabilization of EZH2 by DCAF1/VprBP trigger aberrant gene silencing in colon cancer. *Nature Communications* **14**, 2140.

Gonzalez, M., Moore, H., Li, X. and Kleer, C. (2014). EZH2 expands breast stem cells through activation of NOTCH1 signaling. *PNAS* **111**, 3098-3103.

Grindheim, J., Nicetto, D., Donahue, G. and Zaret, K. (2019). Polycomb repressive complex 2 proteins EZH1 and EZH2 regulate timing of postnatal hepatocyte maturation and fibrosis by repressing genes with euchromatic promoters in mice. *Gastroenterology* **156**, 834-1848.

Han, T., Jiao, F., Hu, H., Yuan, C., Wang, L., Jin, Z., Song, W. and Wang, L. (2016). EZH2 promotes cell migration and invasion but not alters cell proliferation by suppressing E-cadherin, partly through association with MALAT-1 in pancreatic cancer. *Oncotarget* **7**, 11194-11207.

Hanley, C., Noble, F., Ward, M., Bullock, M., Drifka, C., Mellone, M., Manousopoulou, A., Johnston, H., Hayden, A., Thirdborough, S. et al. (2016). A subset of myofibroblastic cancer-associated fibroblasts regulate collagen fiber elongation, which is prognostic in multiple cancers. *Oncotarget* **7**, 6159-6174.

Heo, S. J., Thakur, S., Chen, X., Loebel, C., Xia, B., McBeath, R., Burdick, J. A., Shenoy, V. B., Mauck, R. L. and Lakadamyali, M. (2023). Aberrant chromatin reorganization in cells from diseased fibrous connective tissue in response to altered chemomechanical cues. *Nat Biomed Eng* **7**, 177-191.

Hirukawa, A., Smith, H., Zuo, D., Dufour, C., Savage, P., Bertos, N., Johnson, R., Bui, T., Bourque, G., Basik, M. et al. (2018). Targeting EZH2 reactivates a breast cancer subtype-specific anti-metastatic transcriptional program. *Nature Communications* **9**, 2547.

Hong, L., Williams, N., Jaffe, M., Shields, C. and Haynes, K. (2023). Synthetic reader-actuators targeted to polycomb-silenced genes block triple-negative breast cancer proliferation and invasion. *GEN Biotechnology* **2**, 301-316.

Kalluri, R. and Weinberg, R. (2009). The Basics of Epithelial-Mesenchymal Transition. *J. Clin. Invest.* **119**, 1420–1428.

Kleer, C., Cao, Q., Varambally, S., Shen, R., Ota, I., Tomlins, S., Ghosh, D., Sewalt, R., Otte, A., Hayes, D. et al. (2003). EZH2 is a marker of aggressive breast cancer and promotes neoplastic transformation of breast epithelial cells. *PNAS* **100**, 11606-11611.

Kurokowa, M., Lynch, K. and Podolsky, D. (1987). Effects of growth factors on an intestinal epithelial cell line: transforming growth factor β inhibits proliferation and stimulates differentiation. *Biochemical and Biophysical Research Communications* **142**, 775-782.

Le, H., Ghatak, S., Yeung, C., Tellkamp, F., Günschmann, C., Dieterich, C., Yeroslaviz, A., Habermann, B., Pombo, A., Niessen, C. et al. (2016). Mechanical regulation of transcription controls polycomb-mediated gene silencing during lineage commitment. *Nature Cell Biology* **18**, 864-875.

Le, H., Hill, M., Kollak, I., Keck, M., Schroeder, V., Wirth, J., Skronska-Wasek, W., Schruf, E., Strobel, B., Stahl, H. et al. (2021). An EZH2-dependent transcriptional complex promotes aberrant epithelial remodelling after injury. *EMBO Reports* **22**, e52785.

Lehmann, B., Colaprico, A., Silva, T., Chen, J., An, H., Ban, Y., Huang, H., Wang, L., James, J., Balko, J. et al. (2021). Multi-omics analysis identifies therapeutic vulnerabilities in triple-negative breast cancer subtypes. *Nature Communications* **12**, 6276.

Leight, J., Wozniak, M., Chen, S., Lynch, M. and Chen, C. (2012). Matrix rigidity regulates a switch between TGFβ1-induced apoptosis and epithelial-mesenchymal transition. *Molecular Biology of the Cell* **23**, 781–791.

Levental, I., Levental, K., Klein, E., Assoian, R., Miller, R., Wells, R. and Janmey, P. (2010). A simple indentation device for measuring micrometer-scale tissue stiffness. *J. Phys. Condens. Matter* **22**, 194120.

Liu, F., Mih, J., Shea, B., Kho, A., Sharif, A., Tager, A. and Tschumperlin, D. (2010). Feedback amplification of fibrosis through matrix stiffening and COX-2 suppression. *Journal of Cell Biology* **190**, 693-706.

Lopez, J., Kang, I., You, W., McDonald, D. and Weaver, V. (2011). *In Situ* force mapping of mammary gland transformation. *Integr. Biol (Camb)* **3**, 910-921.

Manning, C., Hooper, S. and Sahai, E. (2015). Intravital imaging of SRF and Notch signalling identifies a key role for EZH2 in invasive melanoma cells. *Oncogene* **34**, 4320-4332.

Martinez-Vidal, L., Murdica, V., Venegoni, C., Pederzoli, F., Bandini, M., Necchi, A., Salonia, A. and Alfano, M. (2021). Causal contributors to tissue stiffness and clinical relevance in urology. *Communications Biology* **4**, 1011.

McMullen, E., Skala, S., Gonzalez, M., Djomehri, S., Chandrashekar, D., Varambally, S. and Kleer, C. (2021). Subcellular localization of EZH2 phosphorylated at T367 stratifies metaplastic breast carcinoma subtypes. *Breast Cancer* **28**, 496-505.

Miranda, T. B., Cortez, C. C., Yoo, C. B., Liang, G., Abe, M., Kelly, T. K., Marquez, V. E. and Jones, P. A. (2009). DZNep is a global histone methylation inhibitor that reactivates developmental genes not silenced by DNA methylation. *Mol Cancer Ther* **8**, 1579-88.

O'Connor, J., Riley, P. N., Nalluri, S. M., Ashar, P. K. and Gomez, E. W. (2015). Matrix rigidity mediates TGFβ1-induced epithelial-myofibroblast transition by controlling cytoskeletal organization and MRTF-A localization. *J. Cell Physiol.* **230**, 1829-1839.

O'Connor, J. W., Mistry, K., Detweiler, D., Wang, C. and Gomez, E. W. (2016). Cell-cell contact and matrix adhesion promote alphaSMA expression during TGFbeta1-induced epithelial-myofibroblast transition via Notch and MRTF-A. *Sci Rep* **6**, 26226.

Pang, J., Toy, K., Griffith, K., Awuah, B., Quayson, S., Newman, L. and Kleer, C. (2012). Invasive breast carcinomas in Ghana: high frequency of high grade, basal-like histology and high EZH2 expression. *Breast Cancer Research and Treatment* **135**, 59-66.

Plodinec, M., Loparic, M., Monnier, C., Obermann, E., Zanetti-Dallenbach, R., Oertle, P., Hyotyla, J., Aebi, U., Bentires-Alj, M., Lim, R. Y. et al. (2012). The nanomechanical signature of breast cancer. *Nature Nanotechnology* **7**, 757-765.

Provenzano, P., Eliceiri, K., Campbell, J., Inman, D., White, J. and Keely, P. (2006). Collagen reorganization at the tumor-stromal interface facilitates local invasion. *BMC Med* **4**.

Roy, A., Basak, N. and Banerjee, S. (2012). Notch1 intracellular domain increases cytoplasmic EZH2 levels during early megakaryopoiesis. *Cell Death and Disease* **3**, e380.

Sankhe, C., Sacco, J. and Gomez, E. (2023). Biophysical Regulation of TGFβ Signaling in the Tumor Microenvironment. In *Engineering and Physical Approaches to Cancer. Current Cancer Research*, (eds I. Wong and M. Dawson), pp. 159-200: Springer, Cham.

Sankhe, C., Sacco, J., Lawton, J., Fair, R., Soares, D., Aldahdooh, M., Gomez, E. and Gomez, E. (2024). Breast cancer cells exhibit mesenchymal-epithelial plasticity following dynamic modulation of matrix stiffness. *Advanced Biology*, 2400087.

Schrader, J., Gordon-Walker, T., Aucott, R., van Deemter, M., Quaas, A., Walsh, S., Benten, D., Forbes, S., Wells, R. and Iredale, J. (2011). Matrix stiffness modulates proliferation, chemotherapeutic response, and dormancy in hepatocellular carcinoma cells. *Hepatology* **53**, 1192-1205.

Shechter, D., Dormann, H. L., Allis, C. D. and Hake, S. B. (2007). Extraction, purification and analysis of histones. *Nature Protocols* **2**, 1445-1457.

Shen, X., Liu, Y., Hsu, Y., Fujiwara, Y., Kim, J., Mao, X., Yuan, G. and Orkin, S. (2008). EZH1 mediates methylation on histone H3 lysine 27 and complements EZH2 in maintaining stem cell identity and executing pluripotency. *Molecular Cell* **32**, 491-502.

Simon, J. and Lange, C. (2008). Roles of EZH2 histone methyltransferase in cancer epigenetics. *Mutation Research/Fundamental and Molecular Mechanisms of Mutagenesis* **647**, 21-29.

Song, S., Zhang, R., Mo, B., Chen, L., Liu, L., Yu, Y., Cao, W., Fang, G., Wan, Y., Gu, Y. et al. (2019). EZH2 as a novel therapeutic target for atrial fibrosis and atrial fibrillation. *Journal of Molecular and Cellular Cardiology* **135**, 119-133.

Stowers, R., Shcherbina, A., Israeli, J., Gruber, J., Chang, J., Nam, S., Rabiee, A., Teruel, M., Snyder, M., Kundaje, A. et al. (2019). Matrix stiffness induces a tumorigenic phenotype in mammary epithelium through changes in chromatin accessibility. *Nature Biomedical Engineering* **3**, 1009-1019.

Su, I.-H., Dobenecker, M., Dickinson, E., Oser, M., Basavaraj, A., Marqueron, R., Viale, A., Reinberg, D., Wülfing, C. and Tarakhovsky, A. (2005). Polycomb group protein EZH2 controls actin polymerization and cell signaling. *Cell* **121**, 425-436.

Tripathi, B., Anderman, M., Bhargava, D., Boccuzzi, L., Qian, X., Wang, D., Durkin, M., Papageorge, A., de Miguel, F., Politi, K. et al. (2021). Inhibition of cytoplasmic EZH2 induces antitumor activity through stabilization of the DLC1 tumor suppressor protein. *Nature Communications* **12**.

Tse, J. and Engler, A. (2010). Preparation of Hydrogel Substrates with Tunable Mechanical Properties. In *Current Protocols in Cell Biology*, vol. 47: John Wiley and Sons Inc.

Tsou, P., Campbell, P., Amin, M., Colt, P., Miller, S., Fox, D., Khanna, D. and Sawalha, A. (2019). Inhibition of EZH2 prevents fibrosis and restores normal angiogenesis in scleroderma. *Proceedings of the National Academy of Sciences* **116**, 3695-3702.

Varambally, S., Dhanasekaran, S., Zhou, M., Barrette, T., Kumar-Sinha, C., Sanda, M., Ghosh, D., Pienta, K., Sewalt, R., Otte, A. et al. (2002). The polycomb group protein EZH2 is involved in progression of prostate cancer. *Nature* **419**, 624-629.

Walker, C., Batan, D., Bishop, C., Ramirez, D., Aguado, B., Schroeder, M., Crocini, C., Schwisow, J., Moulton, K., Macdougall, L. et al. (2022). Extracellular matrix stiffness controls cardiac valve myofibroblast activation through epigenetic remodeling. *Bioengineering and Translational Medicine* **7**, e10394.

Wang, H., Dembo, M. and Wang, Y. (2000). Substrate flexibility regulates growth and apoptosis of normal but not transformed cells. *American Journal of Physiology Cell Physiology* **279**, C1345-C1350.

Ye, X. and Weinberg, R. (2015). Epithelial-mesenchymal plasticity: a central regulator of cancer progression. *Trends in Cell Biology* **25**, 675-686.

Yomtoubian, S., Lee, S., Verma, A., Izzo, F., Markowitz, G., Choi, H., Cerchietti, L., Vahdat, L., Brown, K., Andreopoulou, E. et al. (2020). Inhibition of EZH2 catalytic activity selectively targets a metastatic subpopulation in triple-negative breast cancer. *Cell Reports* **30**, 755-770.E6.

Young, M., Willson, T., Wakefield, M., Trounson, E., Hilton, D., Blewitt, M., Oshlack, A. and Majewski, I. (2011). ChIP-seq analysis reveals distinct H3K27Me3 profiles that correlate with transcriptional activity. *Nucleic Acids Research* **39**, 7415-7427.

Zhang, Q., Dong, P., Liu, X., Sakuragi, N. and Guo, S. (2017). Enhancer of Zeste homolog 2 (EZH2) induces epithelial-mesenchymal transition in endometriosis. *Scientific Reports* **7**, 6804.

Zhang, Q., Padi, S., Tindall, D. and Guo, B. (2014). Polycomb protein EZH2 suppresses apoptosis by silencing the proapoptotic miR-31. *Cell Death and Disease* **5**, e1486.

Figure legends

Figure 1. EZH2 subcellular localization is regulated by matrix stiffness. (A) Immunofluorescence staining for EZH2 in NMuMG cells cultured on 300 Pa and 6300 Pa substrata and treated with TGFβ1 or a vehicle control. Scale bars: 25 μm. (B) Ratio of nuclear:cytoplasmic EZH2 quantified from immunofluorescence images shown in panel A. Data represent mean ± s.e.m and each data point represents the average nuclear:cytoplasmic ratio of at least 50 cells for 3 independent experiments; *p<0.05, **p<0.01. (C) Western blot for EZH2 from whole cell, cytoplasmic, and nuclear protein extracts of NMuMG cells as a function of matrix stiffness and treatment with TGFβ1 or a vehicle control. Densitometric analysis of western blot shown in panel C quantifying relative (D) whole cell, (E) cytoplasmic, and (F) nuclear EZH2 levels. Relative levels are reported normalized to the control vehicle treated cells cultured on 300 Pa substrata. Data represent mean ± s.e.m and each data point represents relative protein levels for 3 independent experiments; *p<0.05, **p<0.01, ***p<0.001. (G) Western blot for H3K27me3 from NMuMG cells as a function of matrix stiffness and treatment with TGFβ1 or a vehicle control. (H) Densitometric analysis of western blot shown in panel G reporting relative levels of H3K27me3 in comparison to the control vehicle treated cells cultured on 300 Pa substrata. Data represent mean ± s.e.m. and each data point represents relative HeK27me3 levels for 3 independent experiments; *p<0.05, **p<0.01, ***p<0.001.

Figure 2. Matrix stiffness and TGFβ1 regulate phosphorylation of EZH2. (A) Western blot for EZH2 in NMuMG cells cultured on 300 Pa or 6300 Pa substrata treated with TGFβ1 or a vehicle control and incubated with or without alkaline phosphatase. (B) Quantification of the relative change in molecular weight of EZH2 from western blot in panel A. *p<0.05, **p<0.01, ***p<0.001. (C) Western blot for pEZH2-T311 and EZH2 in NMuMG cell cultured on 300 Pa or 6300 Pa substrata treated with TGFβ1 or a vehicle control. (D) Densitometric quantification of western blot shown in panel C. **p<0.01. (E) Immunofluorescence staining for pEZH2-T311 in NMuMG cells cultured on 300 or 6300 Pa substrata and treated with TGFβ1 or a vehicle control. Scale bars: 25 μm. (F) Ratio of nuclear:cytoplasmic pEZH2-T311 levels quantified from immunofluorescence images shown in panel E. ****p<0.0001. (G) Immunofluorescence staining for pEZH2-T367 in NMuMG cells cultured on 300 or 6300 Pa substrata and treated with TGFβ1 or a vehicle control. Scale bars: 25 μm. (H) Ratio of nuclear:cytoplasmic pEZH2-T367 levels quantified from immunofluorescence images shown in panel G. Data for all panels represent mean ± s.e.m. for 3 independent experiments; ****p<0.0001.

Figure 3. Inhibiting EZH2 activity reduces TGFβ1-induced changes in H3K27me3 levels and EMT in cells cultured on stiff substrata. (A) Western blot for H3K27me3 in NMuMG cells cultured on 300 Pa

or 6300 Pa substrata and treated with DZNep or a water control prior to TGFβ1 treatment. (B) Densitometric analysis of western blot shown in panel a. Data represent mean ± s.e.m. and each data point represents relative H3K27me3 levels for 3 independent experiments; *p<0.05; ***p<0.001. (C) Immunofluorescence staining for the epithelial marker E-cadherin (red), the mesenchymal marker αSMA (green), and nuclei (blue) in NMuMG cells as a function of matrix stiffness, DZNep, and TGFβ1 treatment. Scale bars: 25 μm. Quantification of (D) cell spread area and (E) aspect ratio as a function of treatment condition and matrix stiffness. Data points represent measurements from individual cells (>150 per condition) and the mean ± s.e.m. are shown for 3 independent experiments. ****p<0.0001. (F) Quantification of the percentage of cells expressing αSMA from immunofluorescence images shown in panel C. Data represent mean ± s.e.m. and each data point represents 3 independent experiments; ***p<0.001. (G) Western blot for the epithelial marker E-cadherin and the mesenchymal markers αSMA, vimentin, and N-cadherin in NMuMG cells as a function of matrix stiffness, DZNep, and TGFβ1 treatment. Densitometric analysis of western blot shown in panel G for (H) E-cadherin, (I) αSMA, (J) vimentin, and (K) N-cadherin levels. Each data point represents the relative protein level. Data are normalized to the 300 Pa vehicle control treated sample. Data represent mean ± s.e.m. for 3 independent experiments; *p<0.05, **p<0.01, ***p<0.001, ****p<0.0001.

Figure 4. siRNA knockdown of EZH2 attenuates TGFβ1-induced changes in H3K27me3 levels and EMT in cells cultured on stiff substrata. (A) Western blot for EZH2 in NMuMG cells following transfection with a control siRNA and siRNA targeting EZH2. (B) Densitometric analysis of western blot shown in panel A. Data represent mean ± s.e.m. and each data point represents protein levels relative to the Control siRNA sample for 3 independent experiments; ***p<0.001. (C) Western blot for H3K27me3 in NMuMG cells transfected with a control or EZH2 siRNA and as a function of matrix stiffness and TGFβ1 treatment. (D) Densitometric analysis of western blot shown in panel C for relative H3K27me3 levels. Data represent mean ± s.e.m. and each data point represents H3K27me3 protein levels relative to the 300 Pa Control siRNA + Control sample for 3 independent experiments; *p<0.05, **p<0.01, ***p<0.001. (E) Immunofluorescence staining for the epithelial marker E-cadherin (red), the mesenchymal marker αSMA (green), and nuclei (blue) in NMuMG cells transfected with a control or EZH2 siRNA and as a function of matrix stiffness and TGFβ1 treatment. Scale bars: 25 μm. Quantification of (F) cell spread area and (G) aspect ratio as a function of matrix stiffness and treatment condition. Data points represent measurements from individual cells (>150 per condition) and the mean ± s.e.m. are shown for 3 independent experiments. ****p<0.0001. (H) Quantification of the percentage of cells expressing αSMA from immunofluorescence images shown in panel E. Data represent mean ± s.e.m. for 3 independent experiments; ***p<0.001. (I) Western blot for E-cadherin, αSMA, N-cadherin, and vimentin in NMuMG cells transfected with a control or EZH2 siRNA as a function of matrix stiffness and TGFβ1 treatment. Densitometric analysis of western

blot shown in panel I for relative (J) E-cadherin, (K) αSMA, (L) N-cadherin, and (M) vimentin levels. Data represent mean ± s.e.m. for 4 (J) or 3 (K, L, M) independent experiments; *p<0.05, **p<0.01, ***p<0.001.

Figure 5. Inhibiting ROCK signaling with Y27632 attenuates TGFβ1-induced EZH2 nuclear translocation in cells cultured on stiff substrata. (A) Immunofluorescence staining for EZH2 in NMuMG cells cultured on 300 or 6300 Pa substrata and treated with Y27632 or a DMSO control prior to TGFβ1 treatment. Scale bars: 25 μm. (B) Ratio of nuclear:cytoplasmic EZH2 levels quantified from immunofluorescence images shown in panel A. Data represent mean ± s.e.m. for 3 independent experiments; ***p<0.001. (C) Western blot for EZH2 present in cytoplasmic and nuclear protein extracts in NMuMG cells as a function of matrix stiffness, Y27632, and TGFβ1 treatment. Densitometric analysis of western blot shown in panel C quantifying (D) cytoplasmic and (E) nuclear EZH2 protein levels relative to the 300 Pa DMSO + Control sample. Data represent mean ± s.e.m. for 3 independent experiments; *p<0.05, **p<0.01, ***p<0.001. (F) Western blot for H3K27me3 in NMuMG cells as a function of matrix stiffness, Y27632, and TGFβ1 treatment. (G) Densitometric analysis of western blot shown in panel F. Data represent mean ± s.e.m. for 3 independent experiments; **p<0.01; ***p<0.001.

Figure 6. Matrix stiffness and cell contractility regulate EZH2 subcellular localization, H3K27me3 levels, and gene expression in response to TGFβ1.

Figure 1

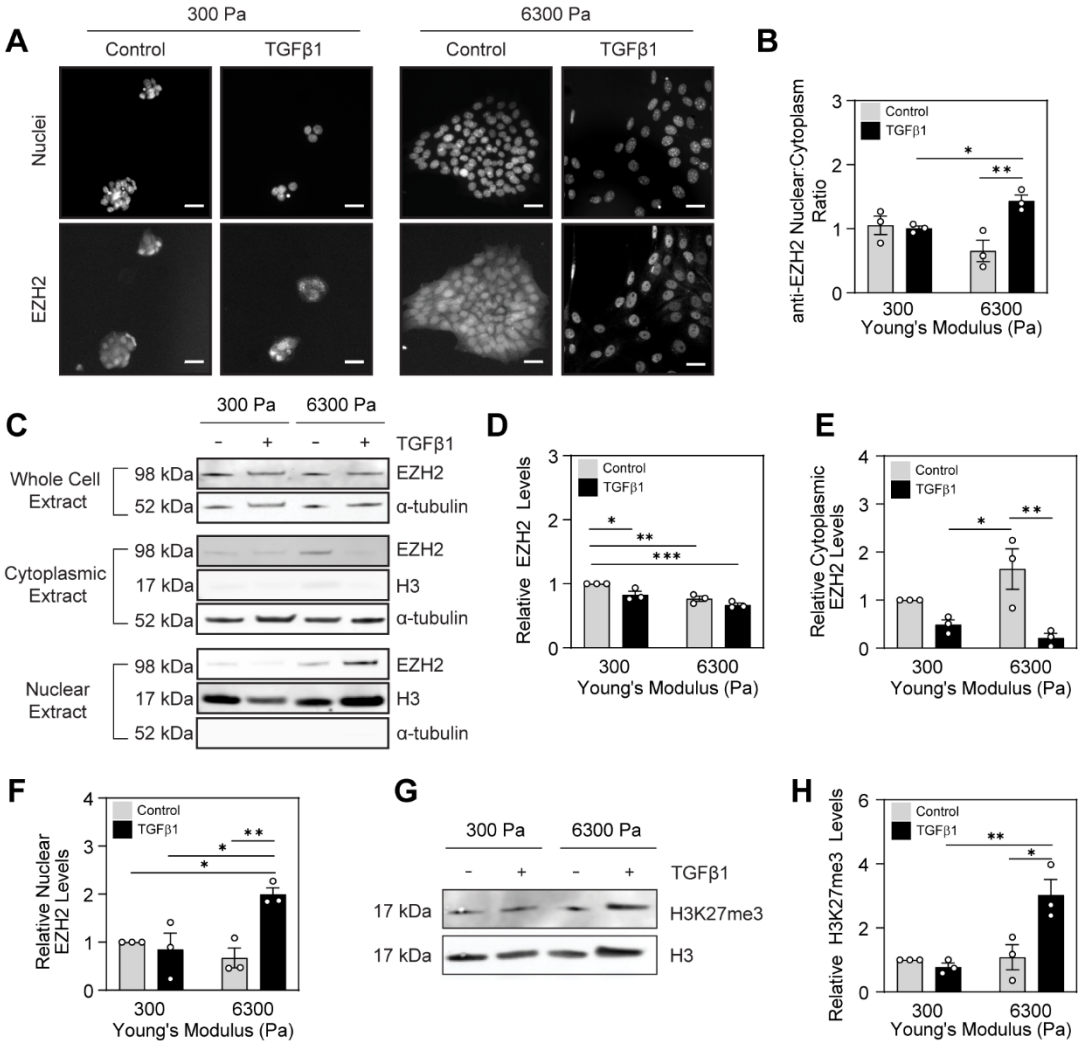
A
300 Pa
6300 Pa
Control
TGFβ1
Control
TGFβ1
Nuclei
EZH2
B
anti-EZH2 Nuclear:Cytoplasm Ratio
Control
TGFβ1
300
6300
Young's Modulus (Pa)
C
300 Pa
6300 Pa
TGFβ1
Whole Cell Extract
98 kDa
EZH2
52 kDa
α-tubulin
Cytoplasmic Extract
98 kDa
EZH2
17 kDa
H3
52 kDa
α-tubulin
Nuclear Extract
98 kDa
EZH2
17 kDa
H3
52 kDa
α-tubulin
D
Relative EZH2 Levels
Control
TGFβ1
300
6300
Young's Modulus (Pa)
E
Relative Cytoplasmic EZH2 Levels
Control
TGFβ1
300
6300
Young's Modulus (Pa)
F
Relative Nuclear EZH2 Levels
Control
TGFβ1
300
6300
Young's Modulus (Pa)
G
300 Pa
6300 Pa
TGFβ1
17 kDa
H3K27me3
17 kDa
H3
H
Relative H3K27me3 Levels
Control
TGFβ1
300
6300
Young's Modulus (Pa)

Figure 2

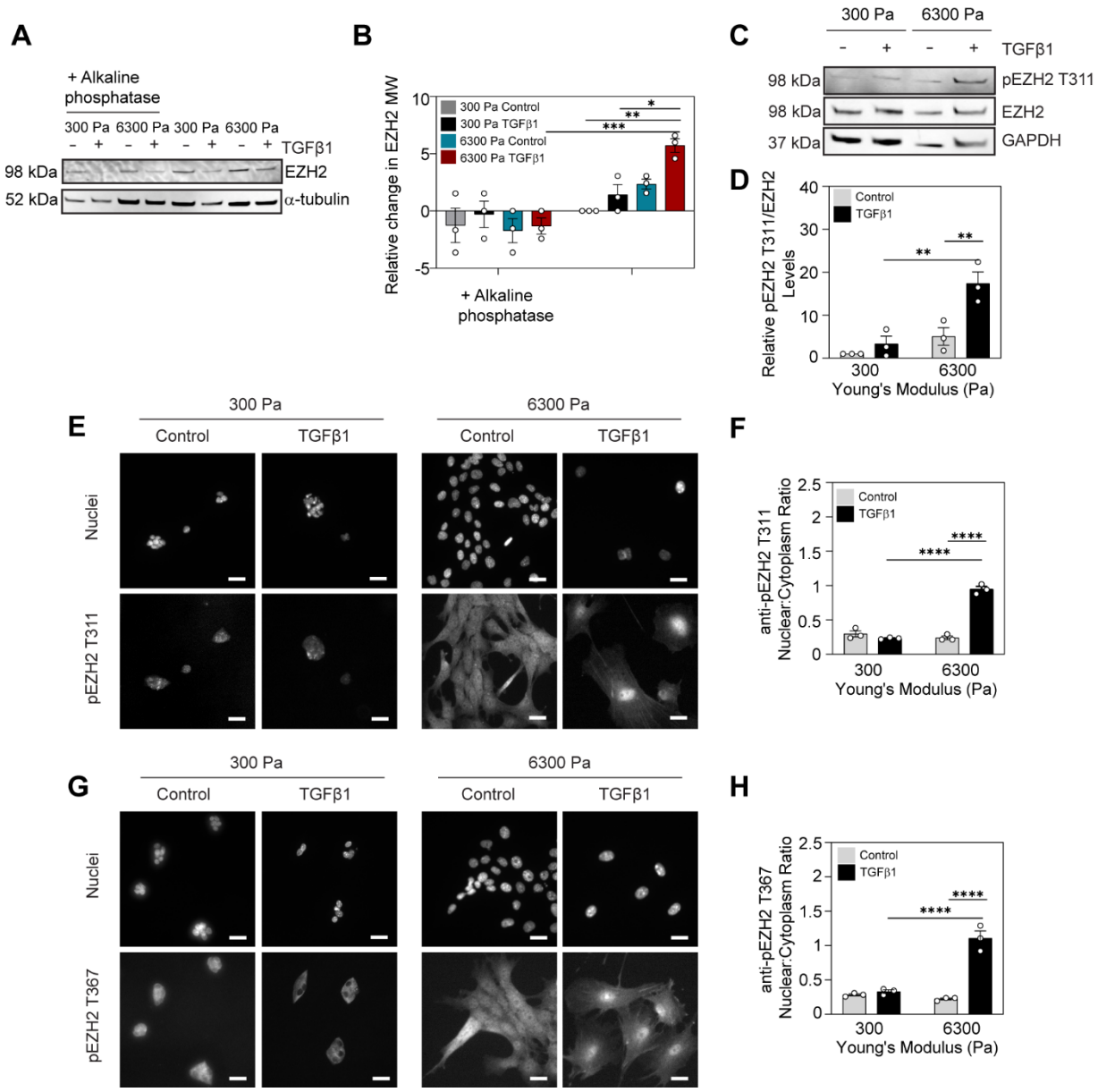
A
+ Alkaline phosphatase
300 Pa 6300 Pa 300 Pa 6300 Pa
- + - + - + - + TGFβ1
98 kDa
EZH2
52 kDa
α-tubulin
B
Relative change in EZH2 MW
300 Pa Control
300 Pa TGFβ1
6300 Pa Control
6300 Pa TGFβ1
+ Alkaline phosphatase
C
300 Pa 6300 Pa
- + - + TGFβ1
98 kDa
pEZH2 T311
98 kDa
EZH2
37 kDa
GAPDH
D
Relative pEZH2 T311/EZH2 Levels
Control
TGFβ1
Young's Modulus (Pa)
E
300 Pa 6300 Pa
Control TGFβ1 Control TGFβ1
Nuclei
pEZH2 T311
F
anti-pEZH2 T311 Nuclear:Cytoplasm Ratio
Control
TGFβ1
Young's Modulus (Pa)
G
300 Pa 6300 Pa
Control TGFβ1 Control TGFβ1
Nuclei
pEZH2 T367
H
anti-pEZH2 T367 Nuclear:Cytoplasm Ratio
Control
TGFβ1
Young's Modulus (Pa)

Figure 3

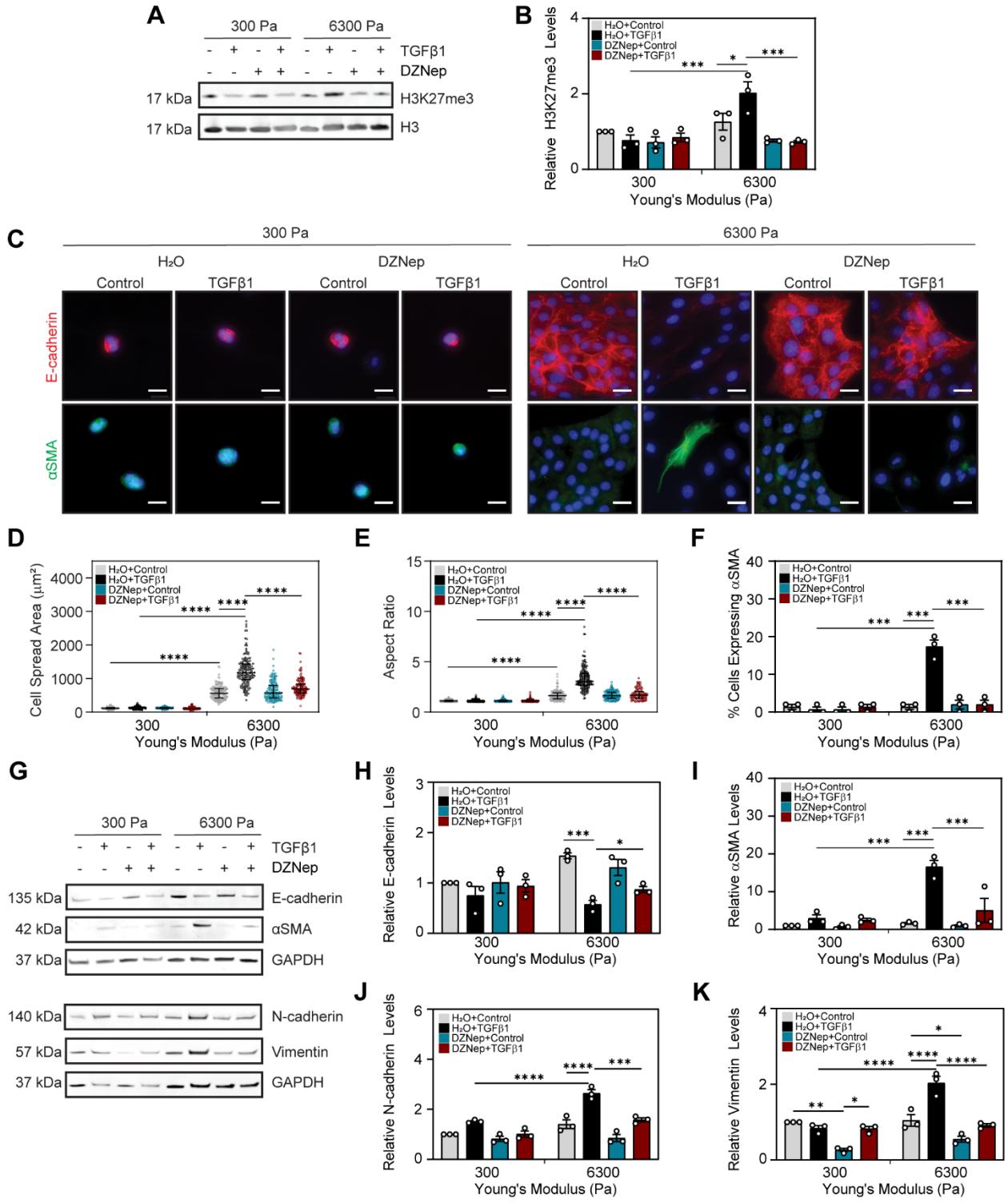
A
300 Pa
6300 Pa
TGFβ1
DZNep
17 kDa
H3K27me3
17 kDa
H3
B
Relative H3K27me3 Levels
H₂O+Control
H₂O+TGFβ1
DZNep+Control
DZNep+TGFβ1
Young's Modulus (Pa)
C
300 Pa
6300 Pa
H₂O
DZNep
Control
TGFβ1
E-cadherin
αSMA
D
Cell Spread Area (μm²)
E
Aspect Ratio
F
% Cells Expressing αSMA
G
135 kDa
E-cadherin
42 kDa
αSMA
37 kDa
GAPDH
140 kDa
N-cadherin
57 kDa
Vimentin
37 kDa
GAPDH
H
Relative E-cadherin Levels
I
Relative αSMA Levels
J
Relative N-cadherin Levels
K
Relative Vimentin Levels

Figure 4

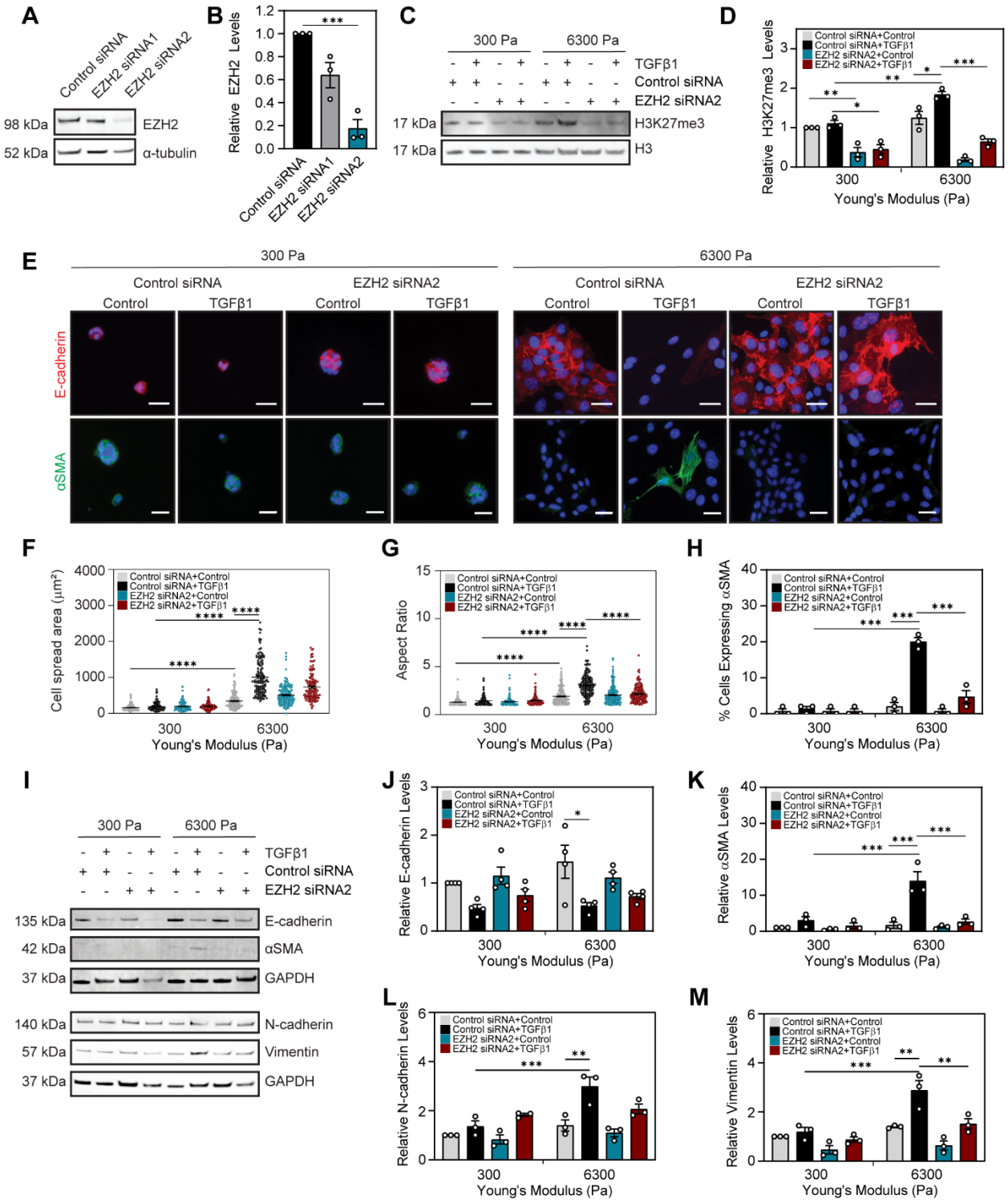
A
Control siRNA
EZH2 siRNA1
EZH2 siRNA2
98 kDa
EZH2
52 kDa
α-tubulin
B
Relative EZH2 Levels
Control siRNA
EZH2 siRNA1
EZH2 siRNA2
C
300 Pa
6300 Pa
TGFβ1
Control siRNA
EZH2 siRNA2
17 kDa
H3K27me3
17 kDa
H3
D
Relative H3K27me3 Levels
Control siRNA+Control
Control siRNA+TGFβ1
EZH2 siRNA2+Control
EZH2 siRNA2+TGFβ1
Young's Modulus (Pa)
E
300 Pa
6300 Pa
Control siRNA
EZH2 siRNA2
Control
TGFβ1
E-cadherin
αSMA
F
Cell spread area (μm²)
Young's Modulus (Pa)
G
Aspect Ratio
Young's Modulus (Pa)
H
% Cells Expressing αSMA
Young's Modulus (Pa)
I
300 Pa
6300 Pa
TGFβ1
Control siRNA
EZH2 siRNA2
135 kDa
E-cadherin
42 kDa
αSMA
37 kDa
GAPDH
140 kDa
N-cadherin
57 kDa
Vimentin
37 kDa
GAPDH
J
Relative E-cadherin Levels
Young's Modulus (Pa)
K
Relative αSMA Levels
Young's Modulus (Pa)
L
Relative N-cadherin Levels
Young's Modulus (Pa)
M
Relative Vimentin Levels
Young's Modulus (Pa)

Figure 5

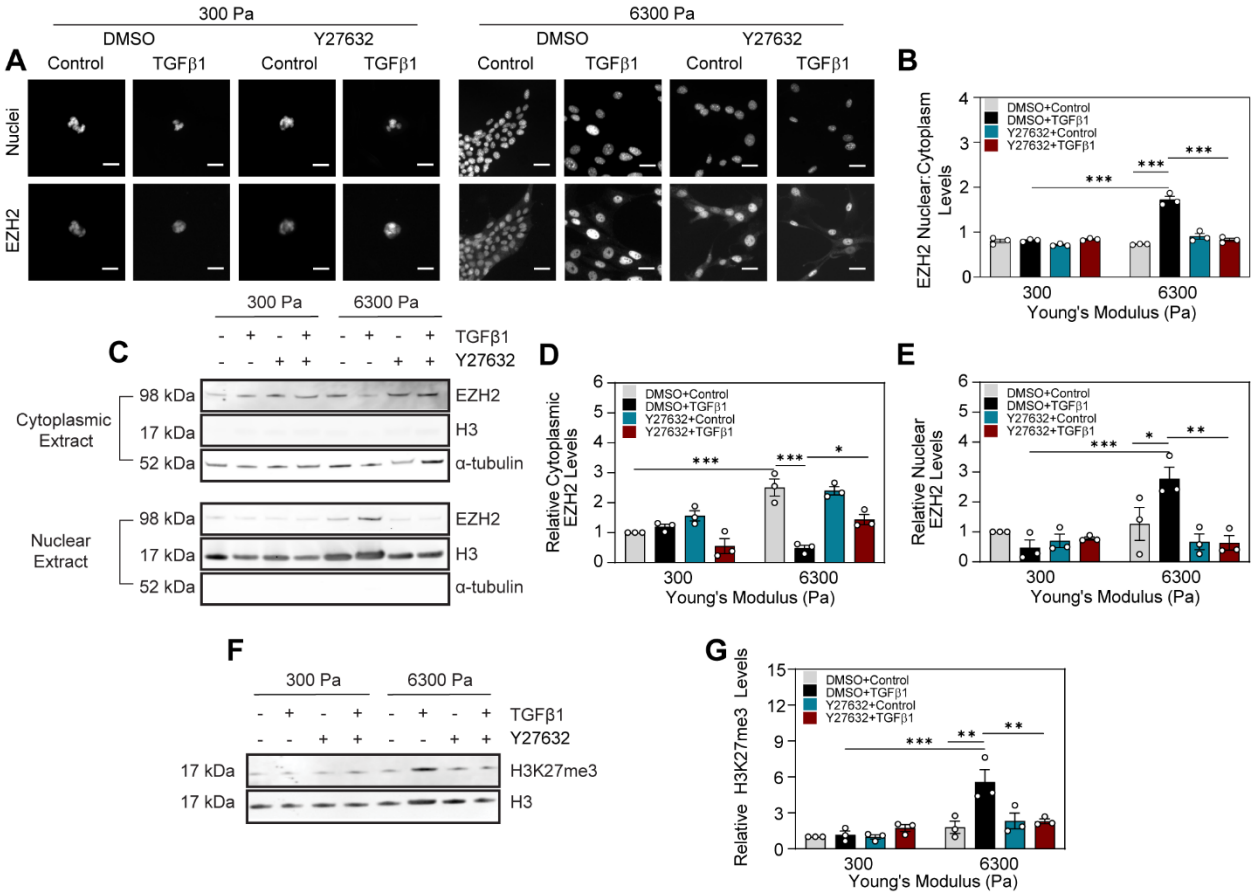
A
300 Pa
6300 Pa
DMSO
Y27632
Control
TGFβ1
Nuclei
EZH2
B
EZH2 Nuclear:Cytoplasm Levels
DMSO+Control
DMSO+TGFβ1
Y27632+Control
Y27632+TGFβ1
Young's Modulus (Pa)
C
TGFβ1
Y27632
Cytoplasmic Extract
Nuclear Extract
98 kDa
17 kDa
52 kDa
EZH2
H3
α-tubulin
D
Relative Cytoplasmic EZH2 Levels
E
Relative Nuclear EZH2 Levels
F
H3K27me3
G
Relative H3K27me3 Levels

Figure 6

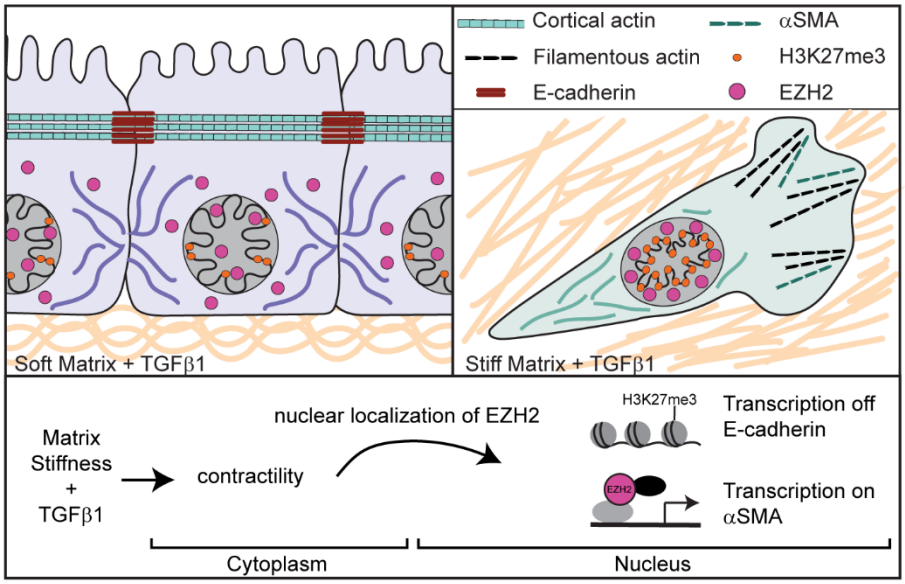
Cortical actin
αSMA
Filamentous actin
H3K27me3
E-cadherin
EZH2
Soft Matrix + TGFβ1
Stiff Matrix + TGFβ1
Matrix Stiffness + TGFβ1
contractility
nuclear localization of EZH2
H3K27me3
Transcription off E-cadherin
EZH2
Transcription on αSMA
Cytoplasm
Nucleus